Available online at www.sciencedirect.com
ScienceDirect
Trans. Nonferrous Met. Soc. China 23(2013) 1737−1750

Transactions of Nonferrous Metals Society of China
www.tnmsc.cn

Application of constitutive and neural network models for prediction of high temperature flow behavior of Al/Mg based nanocomposite

V. SENTHILKUMAR, A. BALAJI, D. ARULKIRUBAKARAN

Department of Production Engineering, National Institute of Technology, Tiruchriappalli 620015, Tamil Nadu, India

Received 13 September 2012; accepted 12 December 2012

Abstract: To predicate the high temperature flow behavior of Al/Mg based nanocomposite, constitutive models such as general flow, Arrhenius hyperbolic, Johnson−Cook(JC) and modified Zerilli−Armstrong (ZA) models, and artificial neural network(ANN) models were developed using stress−strain data collected from hot compression tests carried at different strain rates (0.01−1.0 s^{-1}) and temperatures (523, 623 and 723 K). The validity of the models developed was tested using statistical parameters such as root mean square error (RMSE), regression coefficient (R^2), mean relative error (MRE) and scattered index (I_s). A comparison between ANN and different constitutive models shows that the ANN model has a higher accuracy in estimating the flow stress during hot deformation of AA5083/2%TiC nanocomposite.

Key words: hot compression; Johnson−Cook (JC) model; Modified Zerilli−Armstrong (ZA) model; Arrhenius (AR) hyperbolic model; flow stress; nanocomposite

1 Introduction

Macroscopic and microscopic behaviors of metallic system during thermo-mechanical processing are important to understand the flow and fracture mechanisms during hot deformation. The size, shape and service properties of finished parts are governed by flow path during thermo-mechanical processing [1]. Constitutive equations relate with non-linear relationship that exists among process parameters such as effective stress, effective strain rate and temperature at different levels. These equations that are unique and specific for each material under each processing condition are developed through the use of data obtained under simplified experimental conditions which can be extended to complex situations by well-known hypotheses [2]. The uniaxial hot compression testing is usually employed to provide the necessary data to extract the constitutive equations. Investigations have been carried out in the past and various models to predict the constitutive behaviour in a broad range of metals and alloys [3−6].

A constitutive model involves a number of material constants which are evaluated using a set of experimental data. So, the model developed with all estimated material constants should represent the flow behaviour of the material with adequate accuracy and reliability in a broad range of temperature, strain rate and strain [3]. Different models have been proposed by many researchers; however, general flow equation, Arrhenius (AR) hyperbolic, Johnson−Cook (JC) and Zerilli−Armstrong (ZA) models were used for materials with fairly reasonable accuracy [7−10]. Attempts were made to modify the original models by incorporating adiabatic temperature rise, strain rate sensitivity, temperature sensitivity, strain and strain rate softening, and coupled effects of above parameters [11] for accurate prediction of high temperature and high strain rate flow behaviors. As compared with JC model which necessitates a minimal amount of material constants, ZA model requires more material constants which consider coupled effects of temperature, strain and strain rate, thereby predicting the response of hot deformation in close proximity to that of experimental values. A modified ZA model was developed by SAMANTARAY et al [6] and comparative study was made to evaluate the prediction accuracy of strain rate compensated by Arrhenius equation and JC model with modified ZA model.

The constitutive models developed make use of curve fitting techniques for the determination of material constants from the experimental values which are less accurate and time consuming. As the flow behaviour of material during hot deformation is affected by hardening

Corresponding author: V. SENTHILKUMAR; Tel: +431-2503519; Fax: +431-2500133; E-mail: vskumar@nitt.edu
DOI: 10.1016/S1003-6326(13)62656-4

and softening mechanism, the empirical model developed by experimental values becomes difficult for the performance of theoretical analysis. Means of regression and dependence of strain condition for flow behavior result in a low accuracy of constitutive models. To overcome the above problems, artificial neural network models (ANN) were used to predict flow stress during hot deformation as they can be used to model complex physical phenomenon without invoking mathematical model. ANN model has the capability of performing highly accurate non-linear fit, retaining memory of data and can also adjust the state of network on the basis of original network to adopt new data-sets through training.

LIN et al [12] predicted the flow behaviour of 42CrMo steel using ANN models during hot compression with results having good relation with experimental values. REDDY et al [13] developed a back-propagation neural network model to predict the flow stress of Ti−6Al−4V alloy and pointed out that the network can be successfully trained across different phase regions. They developed the constitutive relationship model for Ti40 alloy and reported that the predicted flow stress by artificial neural network model was in good agreement with experimental results. A three-layer feed forward artificial neural network with a back-propagation learning algorithm was established to explore and predict the flow behavior of 28CrMnMoV steel during hot compression [14]. LIU et al [15] compared the prediction method of flow stress using the Zener−Holloman parameter and hyperbolic sine stress function with ANN model for T1 (W18Cr4V) high-speed steel. CHEN et al [16] compared the prediction method of flow stress using the Zerilli–Armstrong model and ANN model for pure molybdenum. Though ANN model results cannot be directly utilized for developing finite element simulation and analysis during hot deformation, the FEM simulation can be coupled with ANN model for finding the effects of input parameters on process outcome. HANS et al [17] developed forming data using FEM simulation which were subsequently used for training back propogation (BP) ANN model for accurately predicting the metal forming processes. The values predicted were validated using experimental results.

In the present work, isothermally hot compression tests were carried out on AA5083/2%TiC nanocomposite samples under temperatures of 523−723 K and strain rates of 0.01−1.0 s^{-1}, respectively. The experimental flow stress and corresponding input parameters such as strain, strain rate and temperature were used to develop different constitutive models, such as general flow, Arrhenius hyperbolic, JC and modified ZA models. Further, statistical parameters such as mean absolute relative error, correlation coefficient, root mean square error and scattered index were evaluated for each model.

ANN model developed for the prediction of flow stress was compared with various constitutive models using the estimated statistical parameters.

2 Experimental

The AA5083/2%TiC nanocomposite was produced through the P/M route followed by extrusion. The AA5083 powders with average particle size of 30 μm (0.2% Cr, 0.1% Cu, 0.4% Fe, 0.4% Si, 4.5% Mg, 0.4% Mn, 0.15% Ti, 0.25% Zn, balance Al) were blended with 2% (volume fraction) of TiC nano particles (with an average particle size of 37.5 nm) for 2 h without process control agent at 300 r/min using an Insmarts system laboratory scale planetary ball mill. Then, blended powders were milled continuously for 5 h. In order to avoid a significant temperature rise, ball milling was stopped periodically for every 15 min and resumed for 15 min. Sulphur-free Toulene was used as the process control agent to avoid the formation of inter-metallic compound. The milled powder mixture was cold compacted at a pressure of 350 MPa to form billets of 30 mm in diameter and 30 mm in height. The compacted billets were coated with graphite spray and sintered at 773 K for 3 h using argon gas as inert atmosphere to avoid excessive grain growth. Sintered billets were soaked at 723 K for 4 h before extrusion and hot extrusion to produce rods of 12 mm in diameter. Extrusion was carried out without atmosphere control and samples were cooled in air at room temperature. During extrusion anti-seize aerosol was applied which acted as a lubricant and as well as a protective layer to prevent oxidation.

Cylindrical compressive specimens of 10 mm in diameter and 10 mm in height were obtained from hot-extruded material. Specimens were coated with graphite spray lubricant to ensure homogeneous deformation. For examining the behavior of the material, the hot compression tests were carried out up to 40% of engineering strain and then samples were quenched in water. The load—stroke data were converted into true stress—true strain curves using standard equations. Constitutive and ANN models discussed in subsequent sections were developed with the true stress and true strain at different temperatures, strain rates and strains obtained from the above experiments.

3 Results and discussion

3.1 Flow behaviour of AA5083/2%TiC

Figure 1(a) shows the back scattered image of the nanocomposite sample. It shows the presence of micro

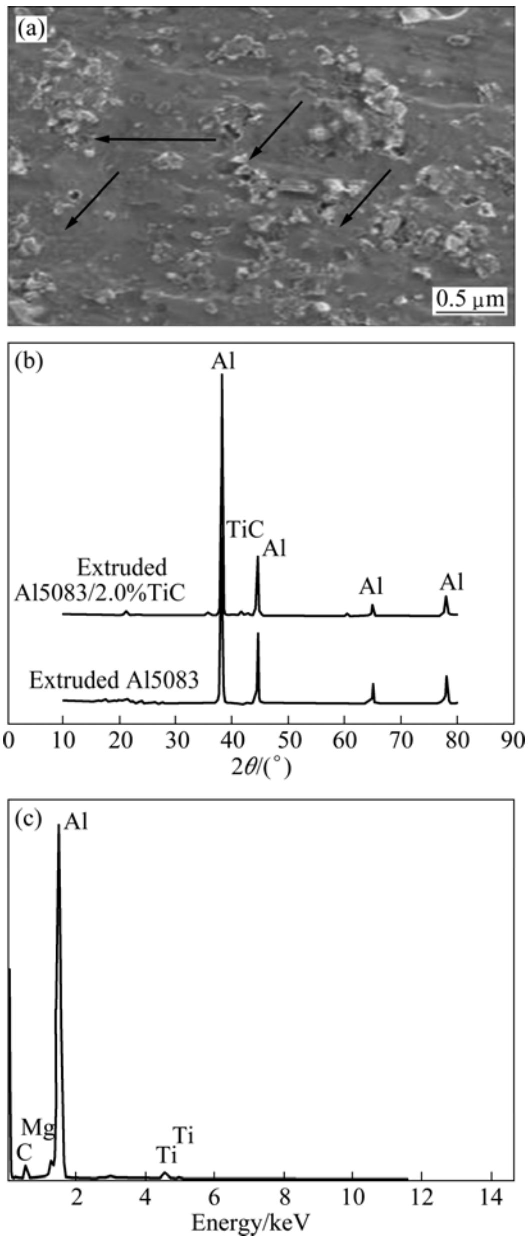

Fig. 1 Back scattered image (a), XRD patters (b) and EDS analysis of as-extruded Al5083/2%TiC nanocomposite (c) (Red arrow indicates micro pores, and orange arrow indicates nano-reinforcements)

pores and distribution of nanoparticle clusters.

Figure 1(b) shows the XRD patterns of alloy and nanocomposite samples. Figure 1(c) shows the EDS analysis. It confirms the presence of Al, Mg, Ti and C in the composite.

Figure 2 shows the typical true stress—strain curves for samples compressed at different temperatures and strain rates. For a given strain level, as the temperature increases, the corresponding stress decreases. Also, for a given strain, the stress increases as the strain rate increases from 0.01 to 1 s^{-1} at all of the temperatures studied. The stress—strain curves appear to flatten out and show a steady but gradual decrease to a strain of 0.5. This indicates the sensitivity of flow stress to the variations of temperature and strain rate. Flow softening behavior was observed at all the temperatures and strain rates. It was observed that the flow softening tendency is greater at lower temperature and higher strain rate. This can be attributed to the rise in temperature, dynamic recrystallization, flow instability, deformation speed, microstructure and adiabatic heating [18,19].

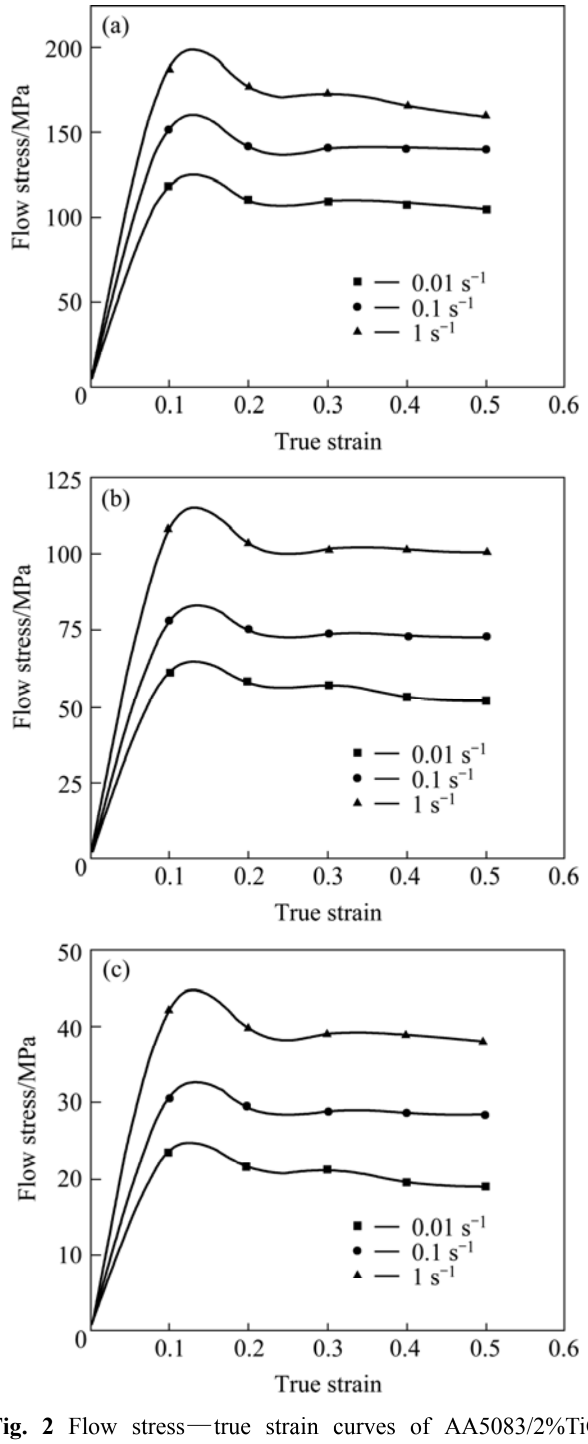

Fig. 2 Flow stress—true strain curves of AA5083/2%TiC nanocomposite at varying strain rates and temperatures of 523 K (a), 623 K (b) and 723 K (c)

3.2 General flow model

A simple constitutive model relating hot deformation parameters such as strain rate and temperature can be expressed as follows:

$$\dot{\varepsilon} = A\sigma^n \exp(-\frac{Q}{RT}) \quad (1)$$

where A and n are material constants; $\dot{\varepsilon}$ is the strain rate; σ is the flow stress; Q is the apparent activation energy of deformation; R is the gas constant; T is the thermodynamic temperature. Figure 3(a) shows the curves between ln σ and ln $\dot{\varepsilon}$ at different temperatures where the slope (n) of the line was obtained. It was observed that the value of n is dependent on strain rate and temperature. For a particular strain level of 0.5, n is found to be 8.48. ln σ and $1/T$ plot was drawn for different strains to find the temperature sensitivity factor s, as shown in Fig. 3(b). The apparent activation energy of the nanocomposite is found taking the average value of slope (s) and n using the following expression:

$$Q=nRs \quad (2)$$

The plots detailed above were drawn in previous work [20] and the activation energy (Q) was found to be 200.84 kJ/mol for a strain of 0.5, which is higher than that for self-diffusion in pure aluminium (142 kJ/mol). The higher Q in the nanocomposite is due to the effect of hard TiC particles in the materials which pin the motion of the dislocations and grain boundaries and raise the deformation resistance. The above calculated activation energy Q was used to estimate temperature compensated strain rate parameter or the Zener–Hollomon parameter (Z) defined as

$$Z = \dot{\varepsilon}\exp(\frac{Q}{RT}) \quad (3)$$

The average Q at a strain of 0.5 is used.

A simple relation of equations (1) and (3) resulted in the following expression:

$$\text{Ln } Z=\ln A+n\ln \sigma \quad (4)$$

The slope of the plot gives a stress exponent value of 8.48, which is close to that obtained in Fig. 3(c). It implies that under the experimental condition considered, the power law relationship for hot deformation is obeyed. Application of above empirical constants n and A into the general flow equation (1) results in the following constitutive model:

$$\dot{\varepsilon}=120.42\sigma^{8.48}\exp[-200840/(8.314T)] \quad (5)$$

The regression coefficients for the plot drawn between ln Z and ln σ shown in Fig. 3(c) are Q, n, s and A at different strain levels (Table 1).

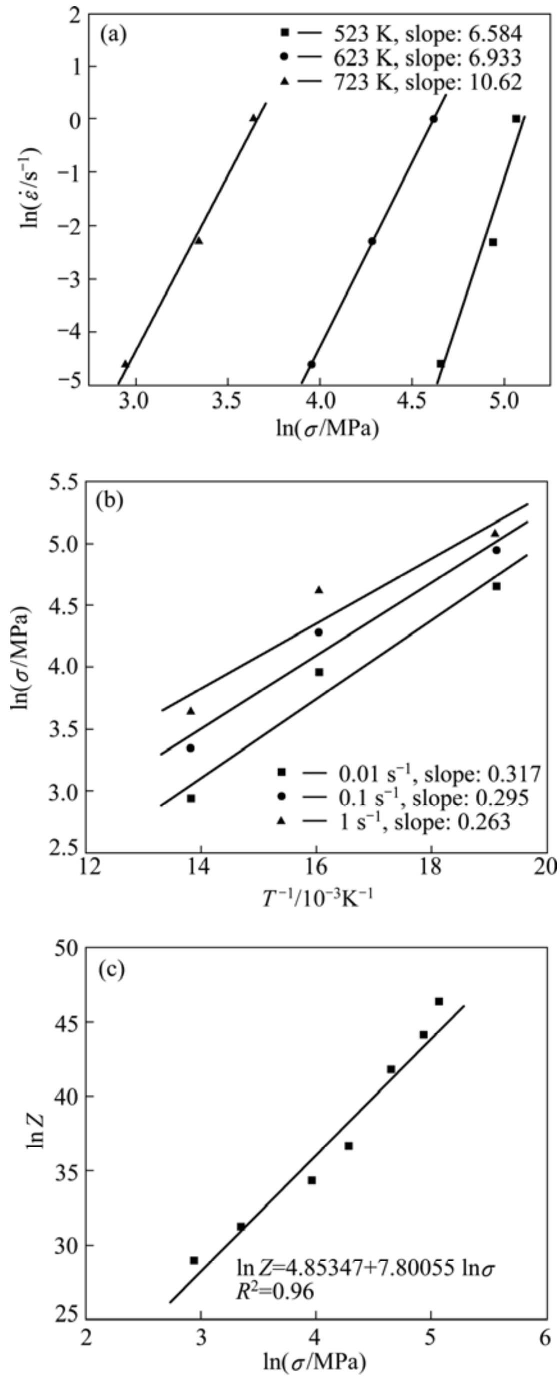

Fig. 3 Variation of flow stress with respect to strain at different temperatures (a), variations of flow stress with respect to temperature at varying strain rates (b), and variation of flow stress with strain compensated Zener−Hollomen parameter for true strain of 0.5 using general flow model (c)

Table 1 Q, $\dot{\varepsilon}$, A, n and s of AA5083/2%TiC nanocomposite

Strain	Q/(kJ·mol^{-1})	A	n	s
0.1	205.91	34.12	8.82	0.27
0.2	204.87	42.52	7.88	0.28
0.3	204.75	53.57	8.02	0.28
0.4	200.97	105.42	8.05	0.28
0.5	200.84	120.42	8.48	0.29

Figure 4 shows the comparison between the experimental and predicted data by general flow model at various processing conditions.

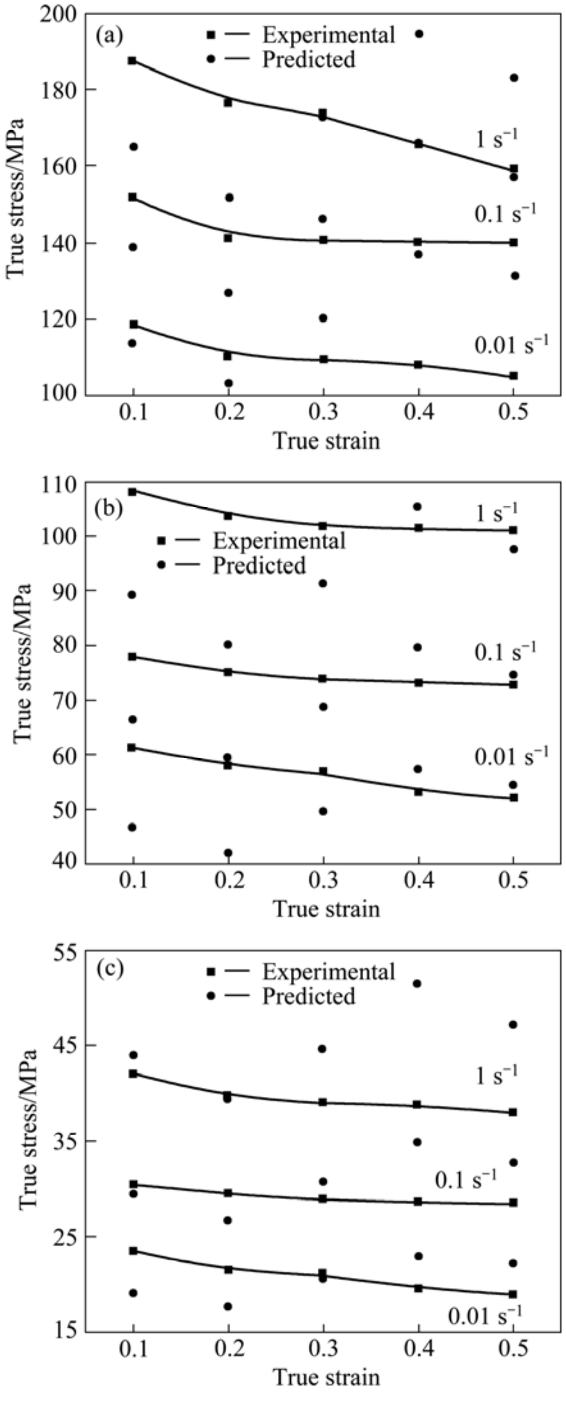

Fig. 4 Comparison between experimental and predicted flow stress using general flow model under strain rates of 0.01−1 s^{-1} at different temperatures: (a) 523 K; (b) 62 3K; (c) 723 K

3.3 Arrhenius hyperbolic model

Arrhenius constitutive model relating various process parameters and material constants with flow stress during hot deformation can be expressed as follows:

$$\dot{\varepsilon} = A[\sinh(\alpha\sigma)]^n \exp(-\frac{Q}{RT}) \tag{6}$$

where α is the stress level; n is the stress exponent constant related to the strain rate.

A detail procedure for the computation of above material constants employing the experimentally measured flow stress was provided in Ref. [21].

Figure 5 shows the relationships among strain rate, temperature and flow stress for the determination of various parameters such as α, n and s. Since, $\ln\dot{\varepsilon}$ is linear with ln[sinh($\alpha\sigma$)], the relationship between the flow stress and strain rate of AA5083/2%TiC nanocomposite fits a hyperbolic sine relation.

The stress exponents n calculated from the slope of the $\ln\dot{\varepsilon}$—ln[sinh($\alpha\sigma$)] at different temperatures are in the range of 4.688−6.130. The temperature sensitive factor was found with curve fitting values of ln[sinh($\alpha\sigma$)] with $1/T$. This varies from 4.11 to 4.47 at varying strain rates. The regression coefficient was found to be above 0.98. The activation energy for corresponding strain rate, temperature and strain level was estimated by Eq. (8).

The activation energy of AA5083/2%TiC for a strain of 0.5 is found to be 185.85 kJ/mol which is significantly higher than the activation energy for self-diffusion of pure aluminium which is 142 kJ/mol.

The correlation coefficient (R^2) for the linear regression of ln Z and ln[sinh($\alpha\sigma$)] was found to be 0.984 (Fig. 6). The stress exponent n of 5.05 calculated from the slope of the plot is in consistent and within the range estimated in Fig.5(c), thereby indicating the effectiveness of the Arrhenius hyperbolic equation for the analysis of hot deformation behavior of AA5083/2%TiC nanocomposite.

By determining A, Q, n and α, the flow stress can be estimated from the constitutive equation represented by

$$\dot{\varepsilon} = 6.46\times10^{13}[\sinh(0.01733\sigma)]^{5.05} \exp(\frac{185850}{RT})$$

The activation energy Q, α, n and A for different strain levels are given in Table 2.

Table 2 Q, α, a, A and n values calculated for Arrhenius hyperbolic model

Strain	Q/(kJ·mol^{-1})	α/MPa^{-1}	A	n
0.1	209.07	0.0156	4.31123×10^{15}	5.582
0.2	197.0277	0.0153	3.36628×10^{14}	5.166
0.3	197.6381	0.0156	8.96931×10^{14}	5.518
0.4	187.7599	0.0172	1.90372×10^{14}	5.355
0.5	185.8544	0.0173	6.46494×10^{13}	5.051

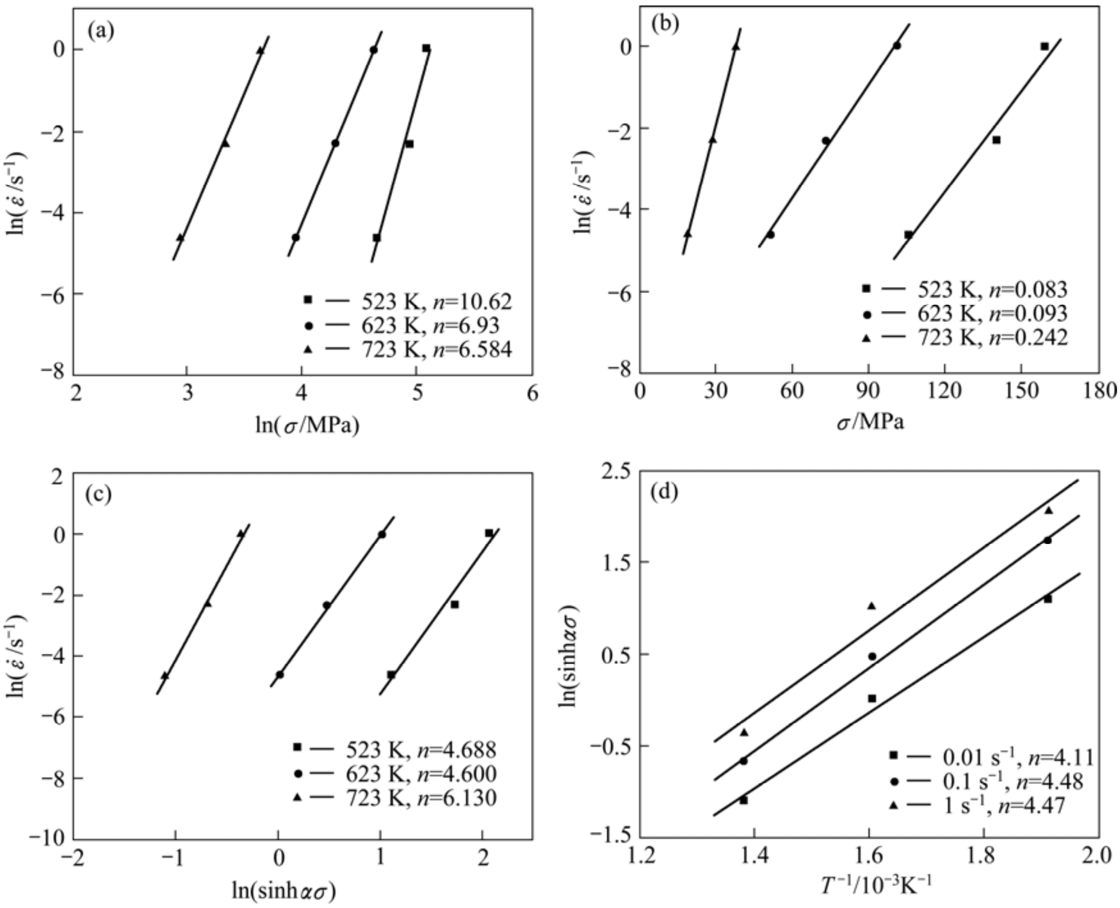

Fig. 5 Plots of $\ln\dot{\varepsilon}$—$\ln\sigma$ (a), $\ln\dot{\varepsilon}$—σ(b), $\ln\dot{\varepsilon}$—ln(sin$\alpha\sigma$) (c) and ln(sinh$\alpha\sigma$)—T^{-1} (d)

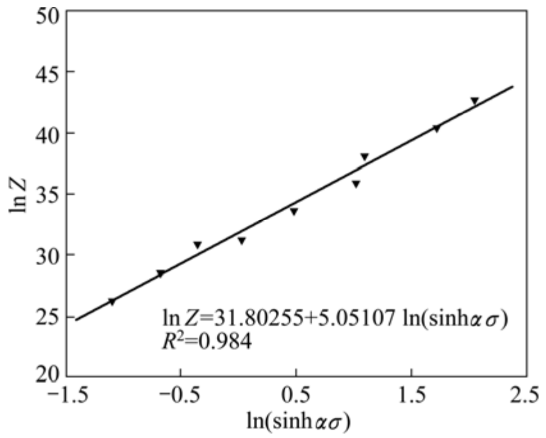

Fig. 6 Variation of flow stress with Zener−Hollomen parameter at true strain of 0.5(Arrhenius model)

Figure 7 shows the relationships between the experimental and predicted data by Arrhenius hyperbolic model at various processing conditions.

3.4 Johnson−Cook model

The original Johnson−Cook model can be expressed as

$$\sigma=(A+B\varepsilon^n)(1+C\ln\dot{\varepsilon}^*)(1-T^{*m}) \quad (7)$$

where A is the yield stress at reference temperature and reference strain rate, here reference temperature (T_r) is the minimum temperature of the experimental temperature (i.e. 523 K) and reference strain rate ($\dot{\varepsilon}_0$) is selected as 1 s^{-1}; B is the coefficient of strain hardening; C is the coefficient of strain rate hardening; $\dot{\varepsilon}^*=\dot{\varepsilon}/\dot{\varepsilon}_0$, is the dimensionless strain rate; T^* is the homologous temperature, $T^*=(T-T_r)/(T_m-T_r)$, where T is the thermodynamic temperature of deformation and T_m is the melting temperature of test material; m is the thermal softening exponent.

The material constant A is found by calculating 0.2% yield stress of the material at reference temperature and strain rate of 1.0 s^{-1}.

The homologous temperature T^* is obtained using the following expression as

$$T^*=(T-T_r)/(T_m-T_r) \quad (8)$$

At temperature of 523 K and strain rate of 1.0 s^{-1} respectively, Eq. (7) is reduced to

$$\sigma=(A+B\varepsilon^n) \quad (9)$$

Taking logarithm on both sides of the above expression, it can be obtained

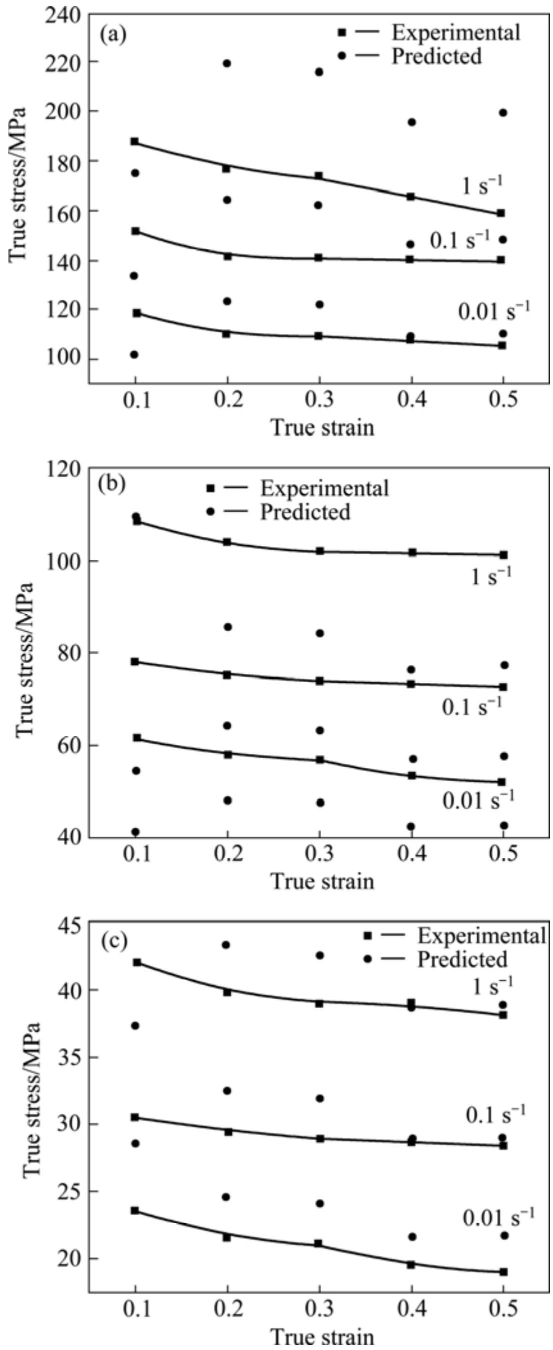

Fig. 7 Relationships between experimental and predicted flow stress using Arrhenius hyperbolic model under strain rates of 0.01 s^{-1}−1 s^{-1} at different temperatures: (a) 523 K; (b) 623 K; (c) 723 K

$$\ln(\sigma - A) = \ln B + n \ln \varepsilon \tag{10}$$

The value of B and strain hardening exponent n can be found by plotting a graph of $\ln(\sigma - A)$ vs $\ln\varepsilon$.

At reference temperature, the homologous temperature term which represents thermal softening effect on the flow stress will be vanished. Eq. (7) can be written as follows:

$$\sigma = (A + B\varepsilon^n)(1 + C \ln \dot{\varepsilon}^*) \tag{11}$$

By taking logarithm on both sides and plotting a graph between $\ln \sigma / (A + B\varepsilon^n)$ and $\ln \dot{\varepsilon}^*$, material constant C can be evaluated.

Finally, the temperature sensitivity, m, can be found at reference temperatures by plotting a graph between $\ln(1-\sigma)/(A + B\varepsilon^n)$ and $\ln T^*$.

For AA5083−2%TiC nanocomposite the material constants are listed in Table 3.

Table 3 Parameters of Johnson−Cook model

C_0/MPa	C_1	C_2	C_3	C_4	C_5	n
156	13.7494	0.0077	−0.0009	0.1051	0.0002	−0.5365

The JC model can be expressed using the material constant as follows:

$$\sigma = (158 + 0.9068\varepsilon^{1.7418})(1 + 0.0731 \ln \dot{\varepsilon}^*)(1 - T^{*0.5145}) \tag{12}$$

Figure 8 shows the comparison of experimental and JC model predicted flow stress for different strains, strain rates and deformation.

3.5 Modified Zerilli−Armstrong model

The ZA model [22] was used for different FCC and BCC materials at different strain states and temperatures between ambient condition and up to $0.6T_m$.

For BCC,

$$\sigma = c_0 + c_1\varepsilon^n[\exp(-c_3T^* + c_4T^* \ln \dot{\varepsilon})] + c_5\dot{\varepsilon}^* \tag{13}$$

For FCC,

$$\sigma = c_0 + c_2\varepsilon^n[\exp(-c_3T^* + c_4T^* \ln \dot{\varepsilon})] \tag{14}$$

where c_0, c_1, c_2, c_3, c_4, c_5 and n are the material constants.

SAMANTARAY et al [6] formulated a modified ZA model incorporating isotropic hardening, temperature softening, strain rate softening, and the coupled effects of strain, strain rate and temperatures.

$$\sigma = c_0 + c_1\varepsilon^n \exp[-(c_2 + c_3\varepsilon)T^* + (c_4 + c_5T^*) \ln \dot{\varepsilon}^*] \tag{15}$$

For computing the material constants used in Eq. (15), reference temperature and reference strain rate were taken as 523 K and 1.0 s^{-1}, respectively.

Applying reference strain rate, Eq. (15) can be written as follows:

$$\sigma = c_0 + c_1\varepsilon^n \tag{16}$$

Taking natural logarithm on both sides, Eq. (16) can be written in the form of linear equation:

$$y=b+ax \tag{17}$$

where slope (a) and intercept (b) in the above expression can be found as reported elsewhere [6].

$$b=\ln(c_0+c_1\varepsilon^n) \tag{18}$$

$$a=-(c_2+c_3\varepsilon) \tag{19}$$

By rearranging the above equation, it can be written

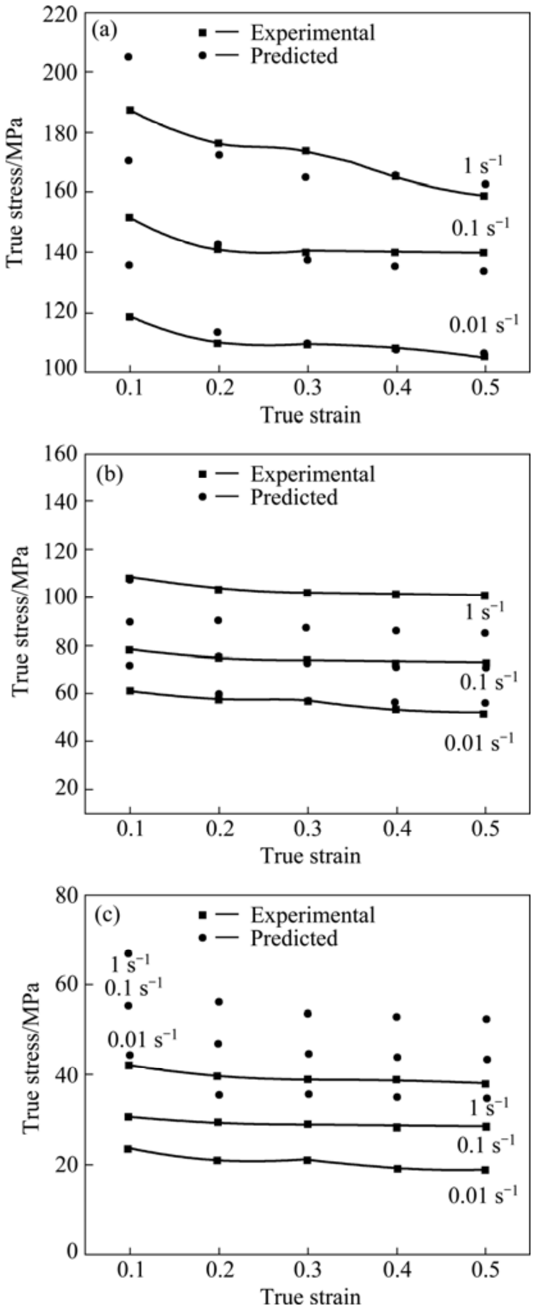

Fig. 8 Comparison between experimental and predicted flow stress using original JC model under strain rates of 0.01−1 s^{-1} at different temperatures: (a) 523 K; (b) 623 K; (c) 723 K

as

$$\ln(\exp b - c_0) = \ln c_1 + n \ln \varepsilon \tag{20}$$

By plotting a graph between $\ln(\exp b - c_0)$ and $\ln\varepsilon$, material constants such as c_1 and n can be calculated.

By plotting a graph between a and ε, the material constants, c_2 and c_3 can be estimated.

As formulated elsewhere [6], the material constants c_4 and c_5 can be estimated by plotting a graph between $\ln\sigma$ and $\ln \dot{\varepsilon}^*$, and following a procedure similar to the evaluation of c_1, c_2, c_3 and n.

In the present case, all the material constants are found and the values are listed in Table 4. Using the material constants estimated in the above procedure, the final modified ZA model can be expressed as follows:

$$\sigma = 156 + 13.74\varepsilon^{-0.5365}[\exp(-(0.0077 - 0.0009\varepsilon)T^* + (0.1051 + 0.0002T^*)\ln \dot{\varepsilon}^*)] \tag{21}$$

Figure 9 shows the comparison between the experimental and predicted data by modified ZA model under various processing conditions.

Table 4 Parameters of modified Zerilli−Armstrong model

A/MPa	B/MPa	C	n	m
158	0.9068	0.0731	1.7148	0.5145

3.6 Neural network model

In the present work, a multi layer perceptron (MLP) based feed-forward neural network back-propagation (BP) algorithm was used which has a good representation power in dealing with complex non-linear problems coupled with multivariable system [14]. The inputs to the neural network model are strain, strain rate and temperature keeping a single output parameter, flow stress. In the case of strain rate $\dot{\varepsilon}$, $\lg \dot{\varepsilon}$ was chosen as a parameter, as it exhibits consistent relationship with flow stress. In this method, the numbers of input and output neurons are equal to the number of input and output parameters respectively and there is one layer including neurons between them. A total number of 45 experiment data collected from hot compression test were used for training and testing the neural network model. According to the MLP BP algorithm, the numbers of input and output neurons are equal to those of input and output parameters respectively, and there is one layer including neurons between them. Different architectures of MLP were used for the calculation of flow stress. All neurons of MLP are connected with the other neurons and the way of connection is forward. As the mentioned earlier, the neural network was trained using the Levenberg−Marquardt algorithm incorporated into the back propagation algorithm. The training function Trainlm has the advantage of the fastest convergence to obtain lower mean square errors than any of the other algorithms tested. The learning is based on gradient descent algorithm and hence requires the activation function to be differentiable. Hence, a logistic sigmoid function expressed as Eq. (22) was employed as the activation function. The transfer functions for both hidden and output layers were performed with Logsig function as the activation function for the flow stress prediction in this study. Because of its simplicity, the Logsig function has become one of the most common and widely used algorithms for solving many real world

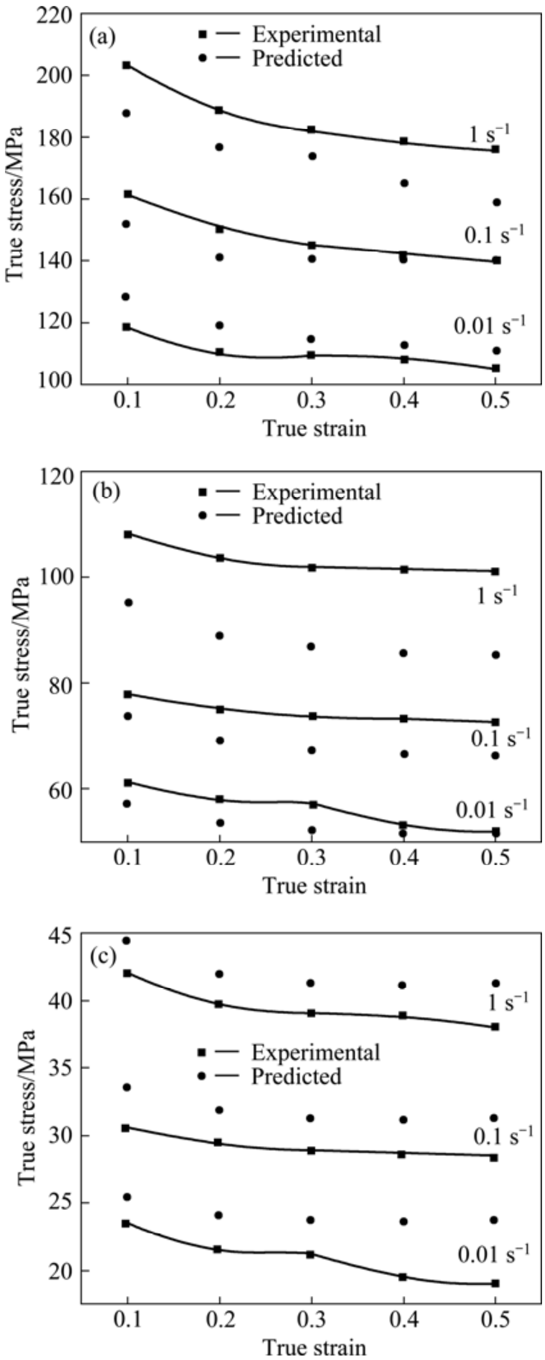

Fig. 9 Comparison between experimental and predicted flow stresses by modified ZA model under strain rates of 0.01−1 s^{-1} at different temperatures: (a) 523 K; (b) 623 K; (c) 723 K

problems as the sigmoid functions are easily differentiable, hence to a certain degree it is transparent to interpretation and analysis. The processing units for computational convenience are employed in the present model:

$$f(x)=1/[1+\exp(-x)] \tag{22}$$

where x is the weighted sum of the input values. The other parameters of MLP architecture and training are listed in Table 5.

Table 5 Training parameters used in neural network

Name of network parameter	Content
Network type	Feed-forward back propagation
Training function	Trainlm
Adaption learning function	Learngdm
Transfer functions for hidden and output layers	Logsig
Performance function	MSE
Training epoch	20000
Goal	0.0001

The neural network toolbox available with MATLAB® version 7.4.0.287 was used to build, train and simulate the network. The numbers of units in input and output layers are dictated by the problem, but the number of hidden units which control the complexity for non-linear problems of the model must be determined. The input–output relationships will specify the objective of the ANN model.

The number of hidden neurons determines the complexity of neural network and precision of predicted values. To determine the number of neurons in the hidden layer, several trains were repeated. After evolving a model with a number of neurons in a hidden layer, the model was tested for statistical parameters such as mean relative error (MRE), root mean square error (RMSE), correlation coefficient (R^2) and scatter index (I_s) using equations as follows:

$$\mathrm{RMSE}=\sqrt{\frac{1}{N}\sum_{i=1}^{N}(E_i-P_i)^2} \tag{23}$$

$$R^2=\sum_{i=1}^{N}(E_i-E_{\mathrm{mean}})(P_i-P_{\mathrm{mean}})\Big/\sqrt{\sum_{i=1}^{N}(E_i-E_{\mathrm{mean}})^2\sum_{i=1}^{N}(P_i-P_{\mathrm{mean}})^2} \tag{24}$$

$$\mathrm{MRE}=\frac{100}{N}\sum_{i=1}^{N}\left|\frac{E_i-P_i}{E_i}\right|\times 100\% \tag{25}$$

$$I_{\mathrm{s}}=\mathrm{RMSE}/E_{\mathrm{mean}} \tag{26}$$

where E is the experimental value and P is the predicted value obtained from the neural network model; E_{mean} and P_{mean} are the mean values of E and P, respectively; N is the total number of data employed in the investigation.

In order to normalize the input and output values within 0−1, the following equation was used for input parameters such as temperature and flow stress:

$$Y_{\mathrm{N}}=\frac{X-0.9X_{\mathrm{Min}}}{1.1X_{\mathrm{Max}}-0.9X_{\mathrm{Min}}} \tag{27}$$

where X is the original temperature, strain and flow stress; X_{Max} and X_{Min} are the maximum and minimum of X, respectively; Y_{N} is the normalized data corresponding to X. However, the normalization method is not appropriate to the data investigated in the present study because strain rate changes significantly and causes too small unified value of $\dot{\varepsilon}_{\text{Max}}$ for the ANN to learn. Therefore, the logarithm method of normalization $\dot{\varepsilon}$ was adopted as follows:

$$\varepsilon_{\text{N}}=\frac{(3+\lg\dot{\varepsilon})-0.9(3+\lg\dot{\varepsilon}_{\text{Min}})}{1.1(3+\lg\dot{\varepsilon}_{\text{Max}})-0.9(3+\lg\dot{\varepsilon}_{\text{Min}})} \tag{28}$$

in which a constant 3 is added so that the normalized data remains positive.

Once the best-trained network is found, all the transformed data convert to their equivalent values, which can be expressed as follows:

$$X=Y_{\text{N}}(1.1X_{\text{Max}}-0.9X_{\text{Min}})+0.9X_{\text{Min}} \tag{29}$$

By employing MLP BP learning algorithm and by evaluating the statistical parameters given in equations (23)−(26), a network with two hidden layers each with two neurons was selected, as shown in Fig. 10, as an optimum model with the best performance. A comparison of different networks tried for the present study, along with performance indicators is listed in Table 6.

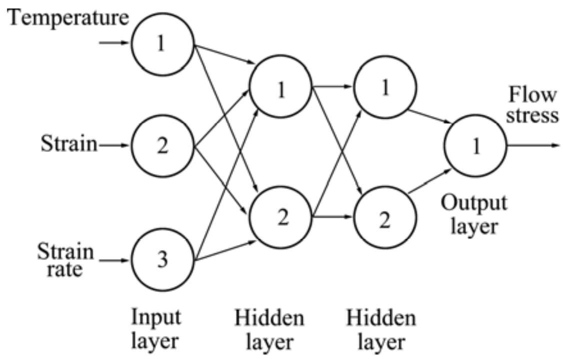

Fig. 10 3-2-2-1 MLP architecture used in ANN model

Table 6 Performance of ANN model for testing datasets of AA5083/2%TiC nanocomposite

Trial No.	Architecture	Number of epochs	MRE	R^2	MRE/%	RMSE/%	I_s
1	3-1-1	NC-20000	0.001863270	0.997	0.333	5.132	0.058
2	3-2-1	NC-20000	0.000564190	0.998	−3.817	6.414	0.072
3	3-3-1	NC-20000	0.000616662	0.989	4.635	7.360	0.083
4	3-4-1	NC-20000	0.000157447	0.926	−35.424	87.298	0.980
5	3-5-1	NC-20000	0.000071935	0.985	8.051	10.254	0.115
6	3-6-1	NC-20000	0.000039900	0.987	−3.242	7.899	0.089
7	3-7-1	NC-20000	0.000012973	0.193	−42.225	92.783	1.041
8	3-8-1	351	5.74×10^{-24}	0.899	−17.394	51.302	0.576
9	3-9-1	82	8.08×10^{-27}	0.974	4.259	11.442	0.128
10	3-10-1	68	4.51×10^{-24}	0.979	6.369	12.929	0.145
11	3-11-1	18	1.48×10^{-30}	0.921	−16.968	52.421	0.588
12	3-12-1	10	4.54×10^{-27}	0.990	−6.102	12.349	0.139
13	3-13-1	22	6.21×10^{-30}	0.978	−21.240	43.874	0.492
14	3-14-1	6	1.11×10^{-28}	0.761	−26.648	31.864	0.358
15	3-15-1	6	8.02×10^{-30}	0.943	−4.289	16.680	0.187
16	3-16-1	6	7.91×10^{-23}	0.875	12.459	30.614	0.344
17	3-17-1	7	7.87×10^{-32}	0.947	−35.966	60.378	0.678
18	3-18-1	7	6.62×10^{-30}	0.935	−3.193	16.769	0.188
19	3-19-1	8	1.70×10^{-30}	0.873	−21.416	23.657	0.266
20	3-20-1	7	1.16×10^{-31}	0.839	−12.843	29.628	0.333
21	3-1-1-1	15	5.18×10^{-2}	0.997	1.515	3.666	0.041
22	3-2-2-1	18	2.48×10^{-4}	0.997	−0.130	3.769	0.042
23	3-3-3-1	15	9.19×10^{-5}	0.998	−1.772	3.452	0.039
24	3-4-4-1	17	6.52×10^{-7}	0.967	−3.017	15.871	0.178
25	3-5-5-1	24	5.60×10^{-27}	0.968	3.895	13.091	0.147
27	3-6-6-1	154	3.59×10^{-23}	0.877	−3.331	31.608	0.355
28	3-7-7-1	8	2.01×10^{-23}	0.994	−0.177	5.259	0.059
29	3-8-8-1	11	1.11×10^{-23}	0.549	−14.393	42.414	0.476
30	3-9-9-1	11	3.37×10^{-26}	0.959	−0.577	20.916	0.235
31	3-10-10-1	8	2.87×10^{-28}	0.932	18.818	23.938	0.269
32	3-11-11-1	14	3.23×10^{-29}	0.937	−29.618	30.210	0.339

Figure 11 shows the comparison between the experimental and predicted flow stress by neural network model under various processing conditions. The statistical parameters evaluated using the neural network model are listed in Table. 7. The selected MLP network with 3-2-2-1 has the highest R^2 of 0.999, and the lowest RMSE, MRE and I_s of 1.326%−0.056%, and 0.016 respectively. After training, 15 testing data were used to validate the accuracy of the proposed MLP network. The result of the testing phase shows that the proposed 3-2-2-1 MLP network using Trainlm and Logsig functions is capable of generalizing between input and output variables with reasonably good prediction errors where the R^2, RMSE, MRE and I_s were estimated as 0.997, 3.769%, −0.009% and 0.042, respectively.

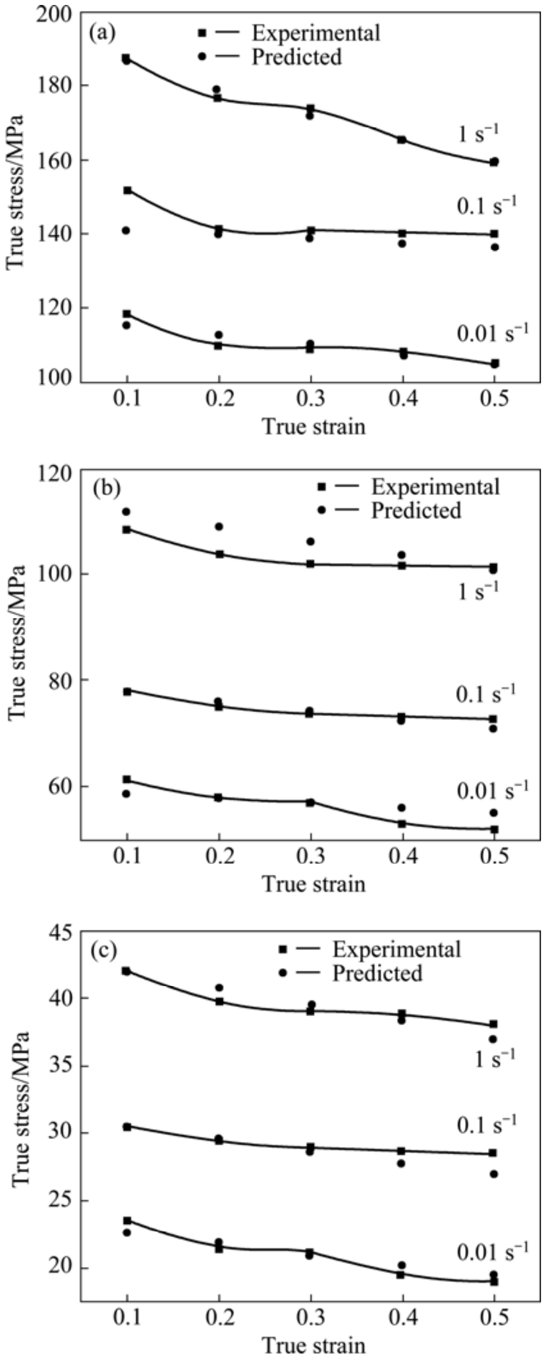

Fig. 11 Comparison between experimental and predicted flow stresses using ANN model at strain rates of 0.01−1 s^{-1}: (a) 523 K; (b) 623 K; (c) 723 K

Table 7 Statistical flow stress values of proposed 3-22-1 network

Flow stress	R^2	RMSE/%	MRE/%	I_s
Training	0.999	1.326	−0.056	0.016
Testing	0.997	3.769	−0.009	0.042

3.7 Comparative studies of constitutive models with ANN model

In order to study the accuracy of constitutive and ANN models to predict the flow stress during hot deformation, as explained in section 3.6, four different statistical parameters, namely correlation coefficient, RMSE, MARE and I_s were evaluated and compared. Figure 12 shows the comparison of experimentally measured and predicted flow stresses using general flow equation, Arrhenius hyperbolic, Johnoson−Cook, modified Zerilli−Armstrong and ANN models. The statistical parameters estimated by different models are listed in Table 8. It is observed that the general flow equation could not predict the flow behavior of AA5083/2%TiC nanocomposite as shown in Fig. 4(a), at high temperatures and higher strain rates. A similar behavior was found for Arhneius hyperbolic model (Fig. 7). However, compared with general flow model, Arrhenius model has better statistical indicators such as R^2, MRE, RMSE and I_s due to more accurate prediction of flow behavior at low and medium temperatures and strain rates. The inability of the above models to predict in the above regions can be attributed to material instability set in the material under these conditions. Activation energies estimated using the above models (Tables 1 and 2) show similar values at initial deformation level, but change substantially as the deformation progresses. As the Arrhenius hyperbolic model has better statistical parameters, it can be suggested for all metallurgical analyses.

Though the general flow and Arrhenius models were used for analysis of hot deformation, their dependence on strain for model development is necessary to develop new constitutive models independent of deformation level (strain). As shown in Figs. 8 and 12(c), JC model has problem in predicting high temperature flow behavior. As shown in Table 8, a poor mean absolute error of 20.58 was obtained in JC model at temperature of 523 K and strain rate of 1 s^{-1} for the estimation of material constants, which was used for other process parameters yield larger error in estimation of flow values. Another disadvantage of JC model as

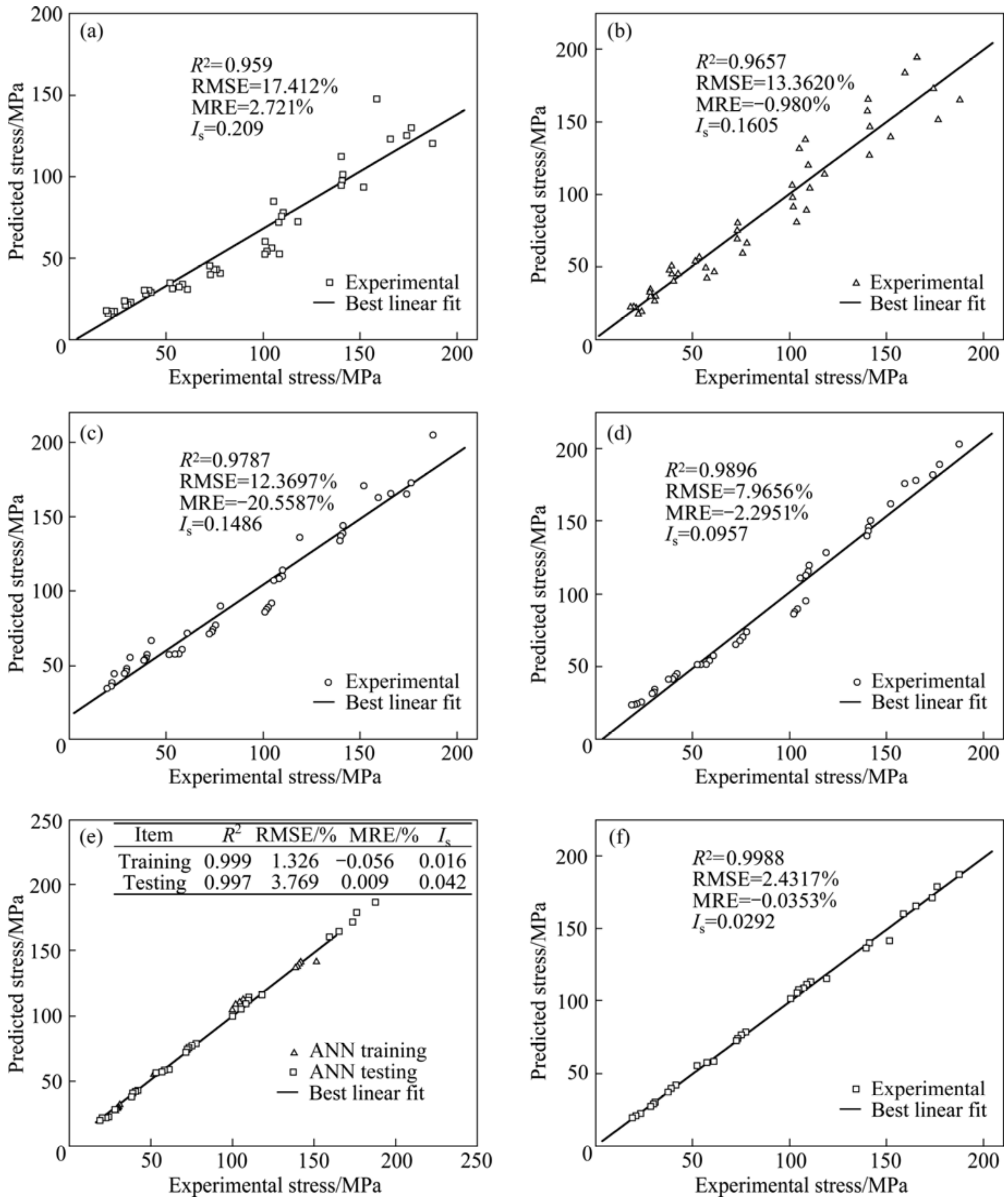

Fig. 12 Comparison of experimental with stresses predicted by general flow model (a), by Arrhenius hyperbolic model (b), by original JC model (c), by modified ZA model (d), by ANN with training and testing data (e) and by full ANN (f)

reported earlier is its appropriation of process parameters such as strain, strain rate and temperature as independent factors and not considering interaction effects among them. The interaction effects of above parameters were considered in the case of modified ZA model, and when this model was applied to flow stress prediction, as shown in Fig. 12(d), better statistical values which are close to those of Arrhenius model were obtained as listed in Table 8.

In the case of 3-2-2-1 neural network model, a maximum absolute error in prediction was found to be 10.533 MPa, which corresponds to the actual flow stress of 101.52 MPa, where the relative error is 6.94%. In another case, when the absolute error is 1.56 MPa, the relative error is 5.49%. This corresponds to the low flow stress of 28.45 MPa. Similarly in another condition, when the absolute error of prediction is −3.24 MPa, the relative error is −6.24%. This corresponds to the high

Table 8 Comparison of experimental flow stress with constitutive and ANN models of AA5083/2%TiC nanocomposite

Model	R^2	RMSE/%	MRE/%	I_s
General flow equation	0.959	17.41	2.721	0.209
Arrhenius hyperbolic model	0.965	13.362	−0.980	0.160
Johnson−Cook model	0.978	12.369	−20.58	0.148
Modified Zerrilli−Armstrong model	0.989	7.965	−2.295	0.095
ANN model	0.999	2.431	−0.035	0.029

flow stress of 52 MPa. In general, it is noticed that the low flow stress is considered to be more sensitive to errors even when the absolute errors are small. This suggests that more uniformity in prediction of flow stress using ANN can be achieved by taking more experimental data pertaining to low flow stress. In addition to the use of logarithmic values of flow stress during normalization, more uniformity in prediction of flow stress during hot deformation can be achieved if more data are taken near the boundaries of the domain [23], and also, more data pertaining to the low flow stress. In the present study, 3-2-2-1 network provides less than ±2% of error in 60% of cases and more than 25% of cases the error falls in the range of ±(2%−4%). The ability of ANN model in predicting the flow behaviour during thermo-mechanical processing can be seen from Figs. 12(e) and (f). The prediction results from the ANN show a higher accuracy than those from the regression constitutive model method as indicated in Table 8.

4 Conclusions

Constitutive models such as general flow, Arrhenius hyperbolic, Johnson−Cook, modified Zerilli−Armstrong models were developed using the experimental data collected from hot isothermal compression under different temperatures and strain rates. Neural network model with 3-2-2-1 multilayer perceptron (MLP) was developed to predict the flow stress of AA5083/2%TiC nanocomposite. The results of the ANN model show satisfactory results with a higher accuracy compared with constitutive model in terms of R^2, MRE, RMSE and I_s. Among the constitutive models developed in the present study, modified Zerilli−Armstrong model shows better statistical indicators of R^2, RMSE and I_s. Arrhenius hyperbolic model shows better mean relative error of −0.980% and can be recommended for estimating metallurgical parameters such as activation energy, strain rate and temperature sensitivity factors.

Acknowledgements

This work was supported by DST-Fast track Scheme (SR/FTP/ETA-69/07), Government of India. The authors are grateful to the Department of Manufacturing Engineering, Annamalai University, Tamil Nadu, India, for extending the facility to conduct experiments.

References

[1] ABBASI S M, SHOKUHFAR A. Prediction of hot deformation behaviour of 10Cr−10Ni−5Mo−2Cu steel [J]. Mater Lett, 2007, 61: 2523−6.

[2] LIN Y C, CHEN M S, ZHANG J. Modeling of flow stress of 42CrMo steel under hot compression [J]. Mater Sci Eng A, 2009, 499: 88−92.

[3] LIN Y C, CHEN X M. A critical review of experimental results and constitutive descriptions for metals and alloys in hot working [J]. Mater Des, 2011, 32: 1733−59.

[4] WANG Z J, QI L H, ZHOU J M, GUAN J T, LIU J. A constitutive model for predicting flow stress of Al18B4O33w/AZ91D composite during hot compression and its validation [J]. Comput Mater Sci, 2011, 50: 2422−6.

[5] CAI J, LI F G, LIU T Y, CHEN B, HE M. Constitutive equations for elevated temperature flow stress of Ti−6Al−4V alloy considering the effect of strain [J]. Mater Des, 2011, 32: 1144−51.

[6] SAMANTARAY D, MANDAL S, BHADURI A K. Constitutive analysis to predict high temperature flow stress in modified 9Cr−1Mo (P91) steel [J]. Mater Des, 2010, 31: 981−984.

[7] STEINBERG D J, COCHRAN S G, GUINAN M W. A constitutive model for metals applicable at high-strain rate [J]. Appl Phys, 1980, 51: 1498−1504.

[8] JOHNSON G R, COO W H. A constitutive model and data for metals subjected to large strains, high strain rates and high temperatures [C]//Proceedings of Seventh International Symposium on Ballistics. The Hague, the Netherlands. 1983, 541−547.

[9] ZERILLI F J, ARMSTRONG R W. Dislocation mechanics based constitutive relations for material dynamics calculations [J]. Appl Phys, 1987, 61: 1816−1825.

[10] FOLLANSBEE P S, KOCKS U F. A constitute description of the deformation of copper based on the use of mechanical threshold stress as internal state variable [J]. Acta Metall, 1988, 36: 81−93.

[11] WANG Yang, ZHOU Yuan-xin, XIA Yuan-ming. A constitutive description of tensile behavior for brass over a wide range of strain rates [J]. Mater Sci Eng A, 2004, 372: 186−190.

[12] LIN Y C, FANG X, WANG Y P. Prediction of metadynamic softening in a multi-pass hot deformed low alloy steel using artificial neural network [J]. Mater Sci, 2008, 43: 5508−5515.

[13] REDDY N S, LEE Y H, PARK C H, LEE C S. Prediction of flow stress in Ti–6Al–4V alloy with an equiaxed [alpha]+[beta] microstructure by artificial neural networks [J]. Mater Sci Eng A, 2008, 492: 276−82.

[14] LI Hong-ying, WEI Dong-dong, LI Yang-hua, WANG Xiao-feng. Application of artificial neural network and constitutive equations to describe the hot compressive behavior of 28CrMnMoV steel [J]. Materials and Design, 2012, 35: 557−562.

[15] LIU Jian-tao, CHANG Hong-bing, Hsu T Y (Xu Zu-yao), RUAN Xue-yu. Prediction of the flow stress of high-speed steel during hot deformation using a BP artificial neural network" [J]. Journal of Materials Processing Technology, 2000, 103(2): 200−205.

[16] CHEN Cheng, YIN Hai-qing, HUMAIL I S, WANG Yu-hui, QU Xuan-hui. A comparative study of a back propagation artificial neural

network and a Zerilli–Armstrong model for pure molybdenum during hot deformation [J]. International Journal of Refractory Metals and Hard Materials, 2007, 25(5−6): 411−416.

[17] HANS R K, RAHUL S S, SANJAY S, PATVARDHAN C. Modeling of manufacturing processes with ANNs for intelligent manufacturing [J]. Machine Tools & Manufacture, 2000, 40: 851−868.

[18] LIN Y C, LIU G. Effects of strain on the workability of a high strength low alloy steel in hot compression [J]. Material Science and Engineering A, 2009, 523(1−2): 139−144.

[19] LIN Y C, CHEN M S, ZHONG J. Micro structural evolution in 42CrMo steel during compression at elevated temperatures [J]. Materials Letters, 2008, 62(14): 2132−2135.

[20] MEDEIROS S C, FRAZIER W G, PRASAD Y V R K. Hot deformation mechanisms in a powder metallurgy nickel-base superalloy IN 625 [J]. Metall Trans A, 2000, 31: 2317−2325.

[21] SENTHILKUMAR V, BALAJI A, ABHISHEK S, HAFEEZ A. Constitutive modelling for the prediction of peak stress in hot deformation processing of Al alloys based nanocomposites [J]. Advanced Materials Research, 2011, 328−330: 1602−1605.

[22] SENTHILKUMAR V, BALAJI A, NARAYANASAMY R. Analysis of hot deformation behaviour of Al 5083–TiC nanocomposite using constitutive and dynamic material models [J]. Materials and Design, 2012, 37: 102−110.

[23] LIN Y C, CHEN Xiao-min. A combined johnson-cook and Zerilli-Armstrong model for hot compressed high-strength steel [J]. Computational Materials Science, 2010, 49: 628−633.

[24] MONTOGOMERY D C. Design and analysis of experiments [M]. New York: John & Sons, 1994.

应用本构模型和神经网络模型预测铝/镁基纳米复合材料的高温流变行为

V. SENTHILKUMAR, A. BALAJI, D. ARULKIRUBAKARAN

Department of Production Engineering, National Institute of Technology, Tiruchriappalli 620015, Tamil Nadu, India

摘　要：为了预测 Al/Mg 基纳米复合材料的高温流变行为，在不同的应变速率(0.01−1.0 s^{-1})和温度(523，623 和 723 K)的条件下进行热压缩试验，利用所得到的应力−应变数据，开发了本构模型，比如一般流动方程。阿累尼乌斯双曲模型、Johnson−Cook(JC)和改性的 Zerilli−Armstrong(ZA)模型及人工神经网络(ANN)模型。通过使用统计参数，例如均方根误差(RMSE)、回归系数(R^2)、平均相对误差(MRE)和分散指数(I_s)，比较了人工神经网络和不同的本构模型。结果表明，人工神经网络模型对 AA5083−2%TiC 复合材料的热变形流动应力的评估准确性更高。

关键词：热压缩；Johnson−Cook (JC)模型；改性 Zerilli−Armstrong(ZA)模型；阿累尼乌斯(AR)双曲模型；流动应力；纳米复合材料

(Edited by Xiang-qun LI)